

Detection of Mitotic Neuroblasts Provides Additional Evidence of Steady-State Neurogenesis in the Adult Small Intestinal Myenteric Plexus

Anastazja M. Gorecki,^{1,2*} Jared Slosberg,^{3*} Su Min Hong,⁴ Philippa Seika,⁴ Srinivas N. Puttapaka,⁴ Blake Migden,⁴ Anton Gulko,⁵ Alpana Singh,⁶ Chengxiu Zhang,⁶ Rohin Gurumurthy,⁶ and Subhash Kulkarni^{4,7,8}

¹Perron Institute for Neurological and Translational Science, Nedlands, Western Australia 6009, Australia, ²School of Biological Sciences, University of Western Australia, Crawley, Western Australia 6009, Australia, ³Department of Genetic Medicine, Johns Hopkins University – School of Medicine, Baltimore, Maryland 21205, ⁴Division of Gastroenterology, Department of Medicine, Beth Israel Deaconess Medical Center, Boston, Massachusetts 02115, ⁵Division of Endocrinology, Department of Medicine, Beth Israel Deaconess Medical Center, Boston, Massachusetts 02115, ⁶Center for Neurogastroenterology, Department of Medicine, Johns Hopkins University–School of Medicine, Baltimore, Maryland 21205, ⁷Division of Medical Sciences, Harvard Medical School, Boston, Massachusetts 02115, and ⁸Program in Neurosciences, Harvard Medical School, Boston, Massachusetts 02115

Abstract

Maintenance of normal structure of the enteric nervous system (ENS), which regulates key gastrointestinal functions, requires robust homeostatic mechanisms, since by virtue of its location within the gut wall, the ENS is subject to constant mechanical, chemical, and biological stressors. Using transgenic and thymidine analog-based experiments, we previously discovered that neuronal turnover—where continual neurogenesis offsets ongoing neuronal loss at steady state—represents one such mechanism. Although other studies confirmed that neuronal death continues into adulthood in the myenteric plexus of the ENS, the complicated nature of thymidine analog presents challenges in substantiating the occurrence of adult neurogenesis. Therefore, it is vital to employ alternative, well-recognized techniques to substantiate the existence of adult enteric neurogenesis in the healthy gut. Here, by using established methods of assessing nuclear DNA content and detecting known mitotic marker phosphor-histone H3 (pH3) in Hu⁺ adult ENS cells, we show that ~10% of adult small intestinal myenteric Hu⁺ cells in mice and ~20% of adult human small intestinal myenteric Hu⁺ cells show evidence of mitosis and hence are cycling neuroblasts. We observe that proportions of Hu⁺ cycling neuroblasts in the adult murine ENS neither vary with ganglionic size nor do they differ significantly between two intestinal regions, duodenum and ileum, or between sexes. Confocal microscopy provides further evidence of cytokinesis in Hu⁺ cells. The presence of a significant population of cycling neuroblasts in adult ENS provides further evidence of steady-state neurogenesis in the adult ENS.

Key words: adult neurogenesis; DNA content; enteric nervous system; flow analyses; neuroblasts; phosphor-histone H3

Significance Statement

Using three-dimensional confocal microscopy, immunohistochemical detection of cell cycle marker phosphor-histone H3, and DNA content assessments using flow cytometry in Hu⁺ cells from adult small intestinal murine myenteric plexus, we show that ~10% of Hu⁺ cells in adult gut are mitotic neuroblasts, whose proportional representation does not significantly differ between sexes or small intestinal regions. We further test and observe mitotic marker pH3 also immunolabels ~23% of adult human myenteric Hu⁺ cells suggesting that the presence of mitotic neuroblasts also extends to the adult human gut. These data further evidence the steady-state adult enteric neurogenesis in the

Received Jan. 2, 2024; revised Dec. 6, 2024; accepted Jan. 9, 2025.

The authors declare no competing financial interests.

Author contributions: A.M.G., J.S., and S.K. designed research; A.M.G., J.S., S.M.H., P.S., S.N.P., B.M., A.G., A.S., C.Z., R.G., and S.K. performed research; A.M.G. contributed unpublished reagents/analytic tools; S.K. analyzed data; J.S. and S.K. wrote the paper.

This work was supported by funding from NIA R01AG66768, R21AG072107, Diacom Foundation (Pilot award Augusta University) and Pilot Grant from the Harvard Digestive Disease Core (S.K.). A.M.G. was supported by a Fulbright Future Scholarship, funded by The Kinghorn Foundation.

Continued on next page.

healthy gut and provide important cellular details in understanding how precursor cells continually generate large numbers of adult neurons in the healthy gut.

Introduction

The cells of the enteric nervous system (ENS) are located entirely within the gut wall and are routinely exposed to significant and continual mechanical, chemical, and biological insults (Gregersen and Kassab, 1996; Sherman et al., 2015; Hyland and Cryan, 2016). Despite these ongoing and significant stressors, the question of how the adult ENS maintains itself has not been adequately addressed, especially given prior reports from multiple groups that a significant proportion of enteric neurons undergo apoptosis at steady state (Nezami et al., 2014; Kozłowska et al., 2016, 2018).

In a previous study, we reported the presence of a neurogenic mechanism, which gives rise to a significant number of new neurons at steady state in the adult gut (Kulkarni et al., 2017). Using thymidine analog studies and multiple lines of evidence to test for neuronal apoptosis, we demonstrated the existence of an adult enteric neurogenic program in the adult murine myenteric plexus (MP) that generates new neurons to replace dying apoptotic neurons, which account for ~10% of all myenteric neurons at any given time. We proposed that this is one mechanism to maintain the structural and functional integrity of the adult ENS, especially in the MP tissue. While other studies provide independent validation of the high rate of neuronal apoptosis in the adult ENS (Chandrasekharan et al., 2011; Nezami et al., 2014; Becker et al., 2018; De Schepper et al., 2018; Ye et al., 2020), the complicated nature of thymidine analog-based assays and their susceptibility to variations in tissue handling and fixation have made it difficult for investigators to consistently detect neurogenesis (Kulkarni and Pasricha, 2022). Thus, there is a need to use alternate methods that can aid in the detection of adult neurogenesis and provide further evidence of a high rate of neurogenesis that counteracts the equally high rate of neuronal apoptosis.

In addition, we also recently showed the presence of significant heterogeneity in myenteric ganglia (Kobayashi et al., 2021; Hamnett et al., 2022). Myenteric ganglia exist in various sizes, as defined by their neuronal numbers, and in the small intestine can contain from 3 to 150 neurons (Kobayashi et al., 2021). The relative distribution of the ganglionic size in the intestine was skewed significantly toward smaller ganglia (i.e., containing fewer neurons; Kobayashi et al., 2021). Similarly, proportions of various neuronal subpopulations contained within these ganglia show significant differences across regions of the intestine (Hamnett et al., 2022). This heterogeneity begs the question of whether the rates of neurogenesis and neuronal loss are equally represented in the diverse ganglia of MP in differing locations in the small intestine and across the two sexes. Since thymidine analog-based assays, which detect the presence of these chemicals dosed to animals over several days, do not permit the study of ongoing neurogenesis at a defined snapshot of time, these assays are unsuitable for providing a real-time assessment of putative differences in neurogenic niches across ganglia and locations. Furthermore, despite high rates of apoptosis (which range from 5 to 30% of all myenteric neurons) reported in human ENS (Chandrasekharan et al., 2011; Kozłowska et al., 2016, 2018), the presence of a neurogenic mechanism in the human ENS is unclear. Since thymidine analogs cannot be administered to human beings, these assays cannot be translated to human tissues, and thus, there is a need to simplify the protocols to facilitate better assessment of neurogenesis both in mice and in human specimens.

To address these issues, in this report, we use three different methods to interrogate whether neurogenesis occurs in adult healthy small intestinal ENS. First, using high-resolution confocal microscopy, we found evidence of binucleated Hu-immunolabeled ganglionic cells in the adult small intestinal MP. Second, by performing a flow cytometry-based estimation of DNA content in myenteric Hu-immunolabeled nuclei, we observe DNA content suggestive of S-phase and G2/M phase in significant proportions of Hu-immunolabeled nuclei—which are indicative of active DNA synthesis and mitosis in a population of adult murine myenteric neurons. Finally, by performing immunostaining with an established mitotic marker phosphor-histone H3 (pH3), we identified the presence of mitotic Hu-immunolabeled cells in the adult murine and human ENS. The proportions of pH3-immunoreactive neurons in the adult murine MP were found to match the previously

J.S. was funded through the Maryland Genetics, Epidemiology, and Medicine training program sponsored by the Burroughs Wellcome Fund and from Walter Benjamin Fellowship (528835020) from Deutsche Forschungsgemeinschaft (P.S.). A.G. and the nuclear isolation at BIDMC was supported by the center grant from NIDDK P30DK135043. We acknowledge the help of Mr. John Tigges, Technical Director/Manager Flow Cytometry Science Center, Beth Israel Deaconess Medical Center, for his help with flow cytometric analyses on FlowJo. We appreciate the help of Dr. Taru Muranen and Dr. Nina Kozlova for their help with FlowJo.

*A.M.G. and J.S. are co-first authors.

Correspondence should be addressed to Subhash Kulkarni at skulkar1@bidmc.harvard.edu.

Copyright © 2025 Gorecki et al. This is an open-access article distributed under the terms of the [Creative Commons Attribution 4.0 International license](https://creativecommons.org/licenses/by/4.0/), which permits unrestricted use, distribution and reproduction in any medium provided that the original work is properly attributed.

observed proportions for apoptotic neurons and were conserved between myenteric ganglia regardless of their size, location in the small intestine, and the sex of the animals. Thus, these three different methods together provide additional evidence of continuous neurogenesis in the adult healthy gut.

Materials and Methods

Animals. Experimental protocols were approved by Johns Hopkins University (JHU) Animal Care and Use Committee and the Animal Care and Use Committee at Beth Israel Deaconess Medical Center (BIDMC) in accordance with the guidelines provided by the National Institutes of Health. Age-matched 2–3-month-old adult wild-type C57BL/6 mice were used. Both male and female mice were used for the pH3-immunostaining experiments, and male mice were used for all the other experiments.

Isolation and immunolabeling of neuronal nuclei from the adult longitudinal muscle–MP (LM–MP) tissue. Mice were anesthetized with isoflurane and killed by cervical dislocation. For small intestinal tissue isolation, a laparotomy was performed, and the entire small intestine was removed and lavaged with PBS containing penicillin–streptomycin (Pen–Strep; Invitrogen). The small intestine was then cut into 1-cm-long segments. Next, tissues were placed over a sterile plastic rod, and a superficial longitudinal incision was made along the serosal surface, and the LM–MP was peeled off from the underlying tissue using a wet sterile cotton swab (Kulkarni et al., 2017) and directly frozen in liquid nitrogen and stored at -80°C for further processing. Two different protocols were used henceforth, which are detailed as follows.

BIDMC protocol: The frozen tissue was next transferred to a gentleMACs C Tube (Miltenyi Biotech) containing 2 ml of TST buffer (containing 60 μl of 5 M NaCl, 42 μl of 1 M MgCl_2 , 20 μl of 1 M Tris–HCl, 2 μl of 1 M CaCl_2 , 10 μl 2% bovine serum albumin (BSA), 6 μl 10% Tween 20, in 1,860 μl ultrapure water), pH 7.5, and allowed to thaw for 2 min. Thawed tissues were chopped using dissecting scissors for 45 s and then added to the C tube, which is installed on the gentleMACs dissociator (Miltenyi Biotech). The tissue was processed through two rounds of 268 rotations, for a total of 72 s dissociation time after which the tube was placed and incubated on ice for 10 min. Next, using a wide-bore, low-retention 1,000 μl pipette tip (Olympus, catalog #23-165RL), the suspension was transferred to a 40 μm prewet cell sieve (Thermo Fisher Scientific, catalog #22-363-547) that was set on top of a sterile 50 ml falcon tube and filtered through. The C tube was washed with 1 ml of 1 \times ST buffer (TST buffer minus BSA and Tween 20), and the buffer was next transferred to the cell sieve. The cell sieve was then washed with 2 ml of 1 \times ST buffer and then discarded. Using again the wide-bore, low-retention 1,000 μl pipette tip (Olympus, catalog #23-165RL), the filtered nuclei suspension was transferred to a prewet 40 μm cell sieve (Thermo Fisher Scientific, catalog #22-363-547) that is set on top of a 5 ml FACS tube. The suspension was spun down in a swing bucket centrifuge at 500 $\times g$ for 5 min and at 4°C . Centrifuge brake was set at half to ensure that the pellet is not disturbed. The top ~ 4.9 ml of the supernatant was removed, and the pellet was washed with 5 ml PBS solution containing 0.02% BSA, which was added to the tube gently, and the tube was again spun at 500 $\times g$ for 5 min and at 4°C . The supernatant was removed, and the nuclear pellet was resuspended in 500 μl of PBS containing 0.02% BSA. The suspension was then split equally into two tubes. The directly conjugated antibody anti-Hu 488 (1:750, Abcam #ab237234; RRID:AB_3668757) was added to the first tube, while the second tube served as the control. A drop of NucBlue (Thermo Fisher Scientific) was added to both the tubes. Both the tubes were incubated on ice for 45 min, after which the nuclear suspensions were spun down at 500 $\times g$ for 5 min and at 4°C , with the centrifuge brakes again set to half. A 450 μl of supernatant from each tube was removed, and the nuclear pellet was resuspended in 450 μl of PBS solution containing 0.02% BSA. The suspensions were then analyzed for NucBlue fluorescence intensity (as a marker for DNA content) in Hu-immunofluorescent nuclei using the CytofLEX flow cytometer.

Johns Hopkins protocol: The frozen and chopped tissue was placed into an ice-cold gentleMACS C tube with 3 ml of TST buffer. The tissue was dissociated on a gentleMACS Octo Dissociator using the 4C_nuclei_01 protocol with prechilled OctoCooler. Disrupted cell suspension was subsequently incubated on ice for 5 min before being filtered through a 40 μm prewet (with 1 \times ST buffer) cell sieve that is set on top of a 50 ml falcon tube. The C tube was rinsed with 1 ml ST buffer, and an additional 2 ml of 1 \times ST buffer was used to rinse the filter. The nuclei suspension was centrifuged in a swing bucket centrifuge at 500 $\times g$ for 5 min and at 4°C with the centrifuge brakes set to half. The pellet was resuspended in 5 ml PBS containing 1% BSA, centrifuged and pelleted again, and finally resuspended in PBS containing 1% BSA and 5% normal goat serum (NGS). This suspension was incubated on ice for 5 min after which the suspension is divided equally into two tubes. Anti-Hu 647 directly conjugated antibody (Abcam, ab237235; RRID:AB_3668731) was added at a concentration of 1:250 to the first but not the second tube, and both the tubes are incubated on ice for 45 min. Excess antibody was removed by washing the suspension twice (again with centrifugation at 500 $\times g$ for 5 min and at 4°C with the centrifuge brakes set to half), and the nuclei suspensions were finally suspended in 1 ml sterile PBS in a 15 ml conical tube. Next, a fixative was freshly prepared by adding 50 μl of 50 mg/ml dithiobis(succinimidyl propionate) in dimethyl sulfoxide solution to 4 ml of ice-cold methanol, dropwise while vortexing at moderate speed. The nuclei suspensions were fixed by adding the freshly prepared fixative dropwise to the nuclei while swirling the suspension to reduce clumping. The fixed nuclei were next incubated at 4°C for 10 min on an end-over-end rotor (speed of 15 rpm). Fixed nuclei were rehydrated by adding two volumes of PBS containing 0.1% Triton X-100 and then washed twice with PBS containing 1% BSA. DAPI was added

to both tubes at a concentration of 1 $\mu\text{g/ml}$, and samples were filtered through a 40 μm before analyses on a flow analyzer (BD FACSAria III).

Flow data was analyzed on FlowJo 10.

Tissue preparation. Mice were anesthetized with isoflurane and killed by cervical dislocation. For small intestinal tissue isolation, a laparotomy was performed, and the entire small intestine was removed and lavaged with PBS containing Pen–Strep (Invitrogen) and then cut into 2-cm-long segments, such that segments from the duodenum, jejunum, and ileum were separated. Next, tissues were placed over a sterile plastic rod, and a superficial longitudinal incision was made along the serosal surface and LM–MP was peeled off from the underlying tissue using a wet sterile cotton swab (Kulkarni et al., 2017) and placed in Opti-MEM medium (Invitrogen) containing Pen–Strep. The tissue was then laid flat and fixed with freshly prepared ice-cold 4% paraformaldehyde (PFA) solution for 4–5 min in the dark. For a small subset of tissues, where we tested how fixation alters immunoreactivity, we fixed LM–MP tissues for 10, 15, and 20 min with freshly prepared ice-cold PFA solution. All LM–MP tissues were fixed within 30 min of euthanasia. After the fixation, the tissue was stored in ice-cold sterile PBS with Pen–Strep for immunofluorescence staining and subsequent microscopy.

Immunocytochemistry. For murine tissue: The fixed LM–MP tissue was washed twice in ice-cold PBS in the dark at 16°C. The tissue was incubated in blocking-permeabilizing buffer (BPB; 5% NGS with 0.3% Triton X-100) for 1 h, followed by incubation with either the combination of (1) anti-pH3 antibody (unconjugated antibody, EMD Millipore, #06-570; RRID:AB_310177, 1:500; conjugated antibody, #3458S, Cell Signaling Technology; 1:250; RRID:AB_10694086) and ANNA-1 (1:1,000; patient antisera against the neuronal Hu antigens; RRID:AB_2813895); (2) anti-cleaved caspase 3 (CC3; #Asp175, Cell Signaling Technology, 1:250; RRID:AB_2070042) and ANNA-1 (1:1,000); (3) anti-PGP9.5 (#ab108986, Abcam, 1:250; RRID:AB_10891773) and ANNA-1 (1:1,000); (4) anti-Hu (#ab184267, Abcam, 1:1,000; RRID:AB_2864321) and ANNA-1 (1:1,000); and (4) anti-Nestin (#NB100-1604, Novus; 1:250; RRID:AB_2282642) and anti-Hu (#ab184267, Abcam, 1:1,000) for 48 h at 16°C in the dark with shaking at 55 rpm. The tissues were then washed three times (15 min wash each) in PBS at room temperature in the dark and incubated in the appropriate secondary antibody (anti-human 488; RRID:AB_2536548; anti-chicken 488; RRID:AB_142924; and anti-rabbit 647; RRID:AB_2535813, Invitrogen, all at 1:500) at room temperature for 1 h while on a rotary shaker (65 rpm). The tissues were again washed three times in PBS at room temperature, counterstained with DAPI to stain the nuclei, overlaid with ProLong Antifade Gold mounting medium, coverslipped, and imaged. ANNA1 patient antiserum was a kind gift from Dr. Sean Pittock at Mayo Clinic.

For formalin fixed paraffin embedded (FFPE) human tissue: The use of the commercially procured human tissue was approved by the Institutional Review Board of BIDMC. FFPE tissue sections from human full-thickness duodenal tissue of four different patients (two males and two females) with no known GI dysmotility disorder were procured from a commercial vendor and from pathology archive BIDMC. To process them, slides were first baked at 55°C for 15 min, after which, they were deparaffinized and rehydrated by immersion through the following solutions: (1) two washes (5 min each) with xylene; (2) two washes with 100% ethanol (5 min each); (3) two washes with 95% ethanol (5 min each); (4) two washes with 70% ethanol (5 min each); and finally (5) two washes with deionized water (5 min each). Next, using sodium citrate buffer, pH 6.0, 40 min antigen retrieval was performed in a pressure cooker. The slides were then cooled in ice-cold 1 \times PBS. Slides were marked with a hydrophobic pen around the sections and then blocked and permeabilized in BPB for 1 h. Buffer was washed off with 1 \times PBS, and sections were incubated with either the combination of directly conjugated anti-pH3 antibody (EMD Millipore, 1:250) and directly conjugated anti-Hu antibody (1:300), or the combination of anti-CC3 (1:250) and ANNA-1 (1:500) for 24 h at 16°C in the dark. For tissue sections treated with anti-CC3 and anti-ANNA1 antibodies, following incubation with primary antibody, the sections were washed three times for 15 min each in PBS at room temperature in the dark and then incubated with the appropriate secondary antibodies (Invitrogen anti-human 488 and anti-rabbit 647; both at 1:500) at room temperature for 1 h. Next, the sections were again washed three times in PBS at room temperature, counterstained with DAPI to stain the nuclei, overlaid with ProLong Antifade Gold mounting medium, coverslipped, and imaged.

Microscopy. Microscopy was performed using the oil immersion 40 \times objective on the Olympus Fluoview 3000rs confocal microscope with galvano and resonance scanning mode, with 40 \times water immersion objective on the Zeiss LSM880, and with 20 \times and 40 \times magnification of the EVOS M7000 microscope. Control tissues that were immunostained with secondary antibodies only were used to set the threshold laser intensities. In mice, all ANNA-1/Hu-immunostained neurons were included in the analysis. Image analyses were performed by using Fiji (NIH) or ImarisViewer (10.2.0).

Results

Hu-expression marks a subset of multinucleated ganglionic cells in adult small intestinal murine myenteric ganglia

Hu-expression is known to be a pan-neuronal marker for all adult enteric neurons (Liu et al., 2009; Desmet et al., 2014; Kulkarni et al., 2017, 2023; D'Errico et al., 2018; Kobayashi et al., 2021). These studies have used both commercially available antibodies against the neuronal Hu antigens (HuB/C/D), as well as the patient-derived ANNA1 sera which contain autoantibodies against the neuronal Hu antigens. As these are often used as alternatives, we tested whether they detected

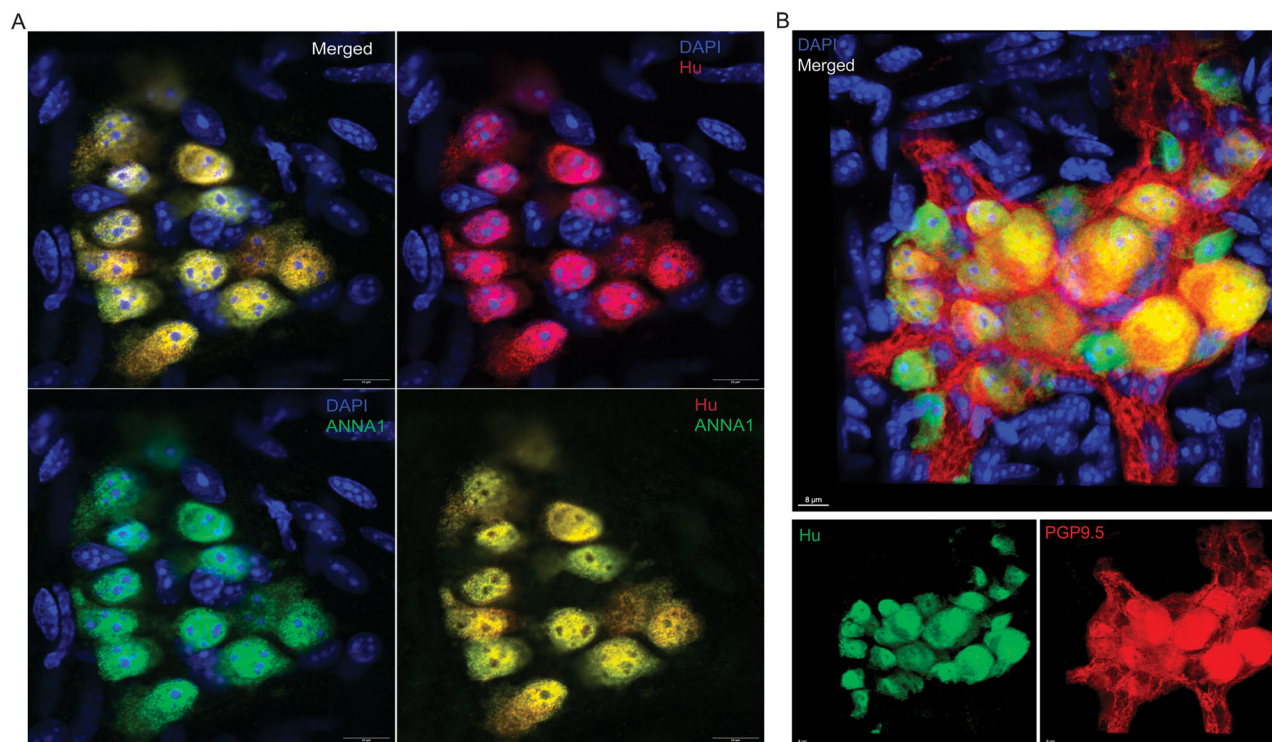


Figure 1. Hu-expression labels all myenteric ganglionic cells that express the pan-neuronal marker PGP9.5. **A**, Representative image (merged and color-segregated) showing coimmunolabeling of an adult murine small intestinal myenteric ganglion with commercially available anti-Hu antibody (red) along with anti-Hu antibodies in the patient-derived ANNA1 antisera (green). Nuclei are labeled with DAPI (blue). Scale bar, 10 μm . **B**, Representative image (merged and panel-segregated) showing coimmunolabeling of an adult murine small intestinal myenteric ganglion with commercially available antibodies against Hu (green) and PGP9.5 (red). Nuclei are labeled with DAPI (blue). Scale bar, 8 μm .

the same ganglionic cells and found by coimmunostaining that the commercially available anti-Hu antibodies detect the same cells as the anti-Hu autoantibodies in the patient-derived ANNA1 antisera (Fig. 1A). Next, we tested the coexpression of Hu and the pan-neuronal marker PGP9.5 and found that Hu immunostaining (ANNA1) colocalized with PGP9.5 immunostaining in the adult murine small intestinal MP (Fig. 1B). By imaging three-dimensional (3D) z-stack of a Hu and PGP9.5-immunostained adult murine small intestinal myenteric ganglia, we found that that some Hu^+ PGP9.5⁺ cells within myenteric ganglia contained more than one nucleus (Fig. 2). This observation was reproduced in tissues from another mouse where two nuclei were observed in a single Hu-expressing cell (Extended Data Fig. 2-1).

About 10% of all adult murine small intestinal myenteric Hu-expressing cells show evidence of more than 2N DNA content by flow cytometry

While binucleated cells suggest impending cytokinesis in a cell (Panet et al., 2015), to further study whether cell cycling occurs in Hu-expressing cells, we first used flow cytometry-based estimation of DNA content in adult murine small intestinal Hu-immunolabeled nuclei to test whether myenteric Hu^+ nuclei show presence of higher than the expected 2N DNA content, which would suggest the presence of cells in S-phase (DNA replication) and in G2/M phase (mitosis) of the cell cycle. On performing this assay on >10,000 unfixed Hu-immunolabeled nuclei derived from LM-MP tissues from adult healthy mice that were housed in the barrier facility at BIDMC, we observed that ~10% of these Hu^+ nuclei show evidence of DNA content greater than expected euploidy (Fig. 3A–C). Based on DNA content, 2.71% of all Hu^+ nuclei were found to be in S-phase, and 7.37% were found to be in G2/M phase of the cell cycle. We next tested whether the observation of >2N DNA content in myenteric Hu^+ nuclei was dependent on fixation or housing conditions. For this, Hu-immunolabeled fixed nuclei that were derived from the small intestinal LM-MP tissue of adult healthy mice housed in a nonbarrier facility at JHU were analyzed and were again found to have 2.61% of all Hu^+ nuclei that were found to be in S-phase, and 7.39% were found to be in G2/M phase of the cell cycle (Fig. 3D; Extended Data Fig. 3-1). Thus, we establish a high degree of concordance in the proportions of Hu^+ cells in S and G2/M phase of cell cycle in adult mice, irrespective of their housing conditions and colony location, as well as whether the nuclei were stained with or without fixation.

About 10% of all adult murine small intestinal myenteric Hu-expressing cells express the cell cycle marker pH3

In addition to flow analyses of Hu-immunolabeled nuclei, we interrogated whether cycling Hu^+ cells can be detected in tissues using a known cell cycling marker. For this, we further tested the presence of mitosis in adult enteric Hu^+ cells by

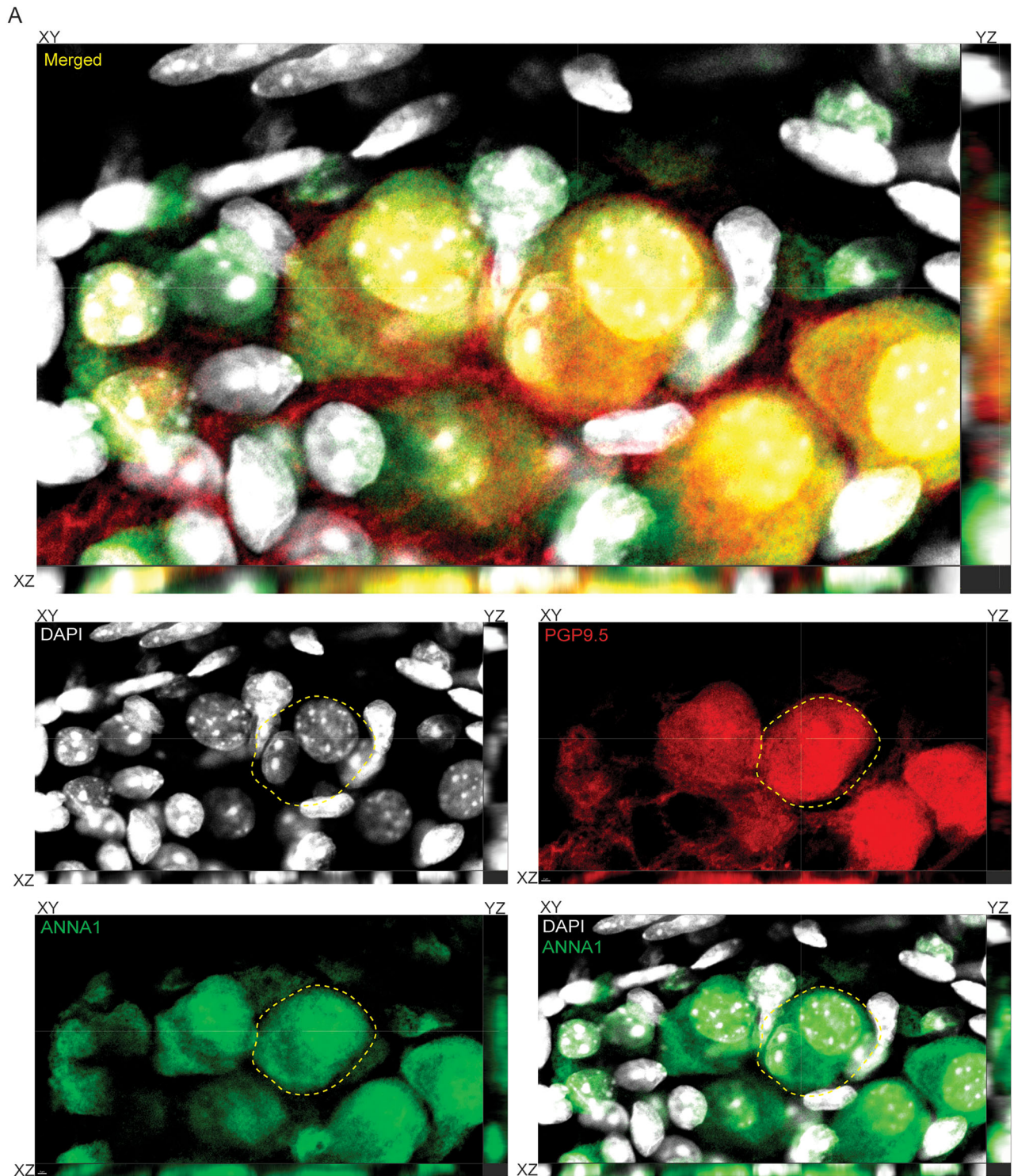


Figure 2. Binucleated ganglionic cells express Hu and PGP9.5. Orthogonal (merged and color-segregated) views of a 3D confocal microscopy image showing that a DAPI-stained- (gray), Hu- (green), and PGP9.5- (red) immunolabeled cell contains two nuclei. XY, YZ, and XY planes of the orthogonal views are denoted for every merged and panel-segregated image. Scale bar, 2 μ m. Additional Hu-immunolabeled binucleated cell with conjoined nuclei is shown in Extended Data Figure 2-1.

microscopic detection of an established mitotic marker pH3 in the neurons of the MP (Kim et al., 2007; Uguen et al., 2015; Tiede et al., 2018; Jiang et al., 2019; Rotelli et al., 2019). By using antibodies against the protein pH3 (phosphorylated at residue Ser10, which occurs at the initiation of the G2 phase and continues into metaphase), we observed that the adult healthy small intestinal LM–MP tissue derived from mice housed in the JHU mouse colony contains diverse cell

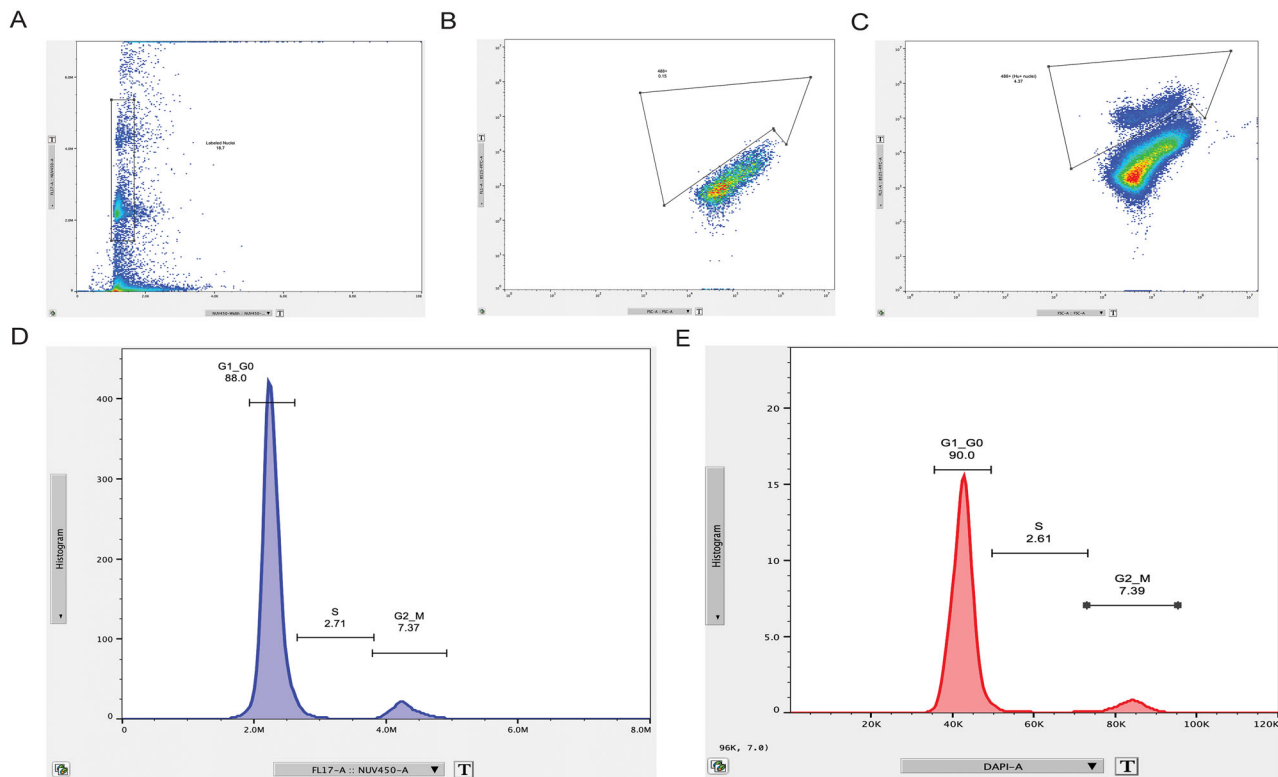


Figure 3. Evidence of S and G2/M phases of cell cycle in a population of Hu-immunolabeled cells from the small intestinal MP tissue of adult healthy mice. Flow analyses of nuclei isolated from the LM–MP tissue from adult healthy mice housed in a barrier facility at BIDMC when immunolabeled with directly conjugated anti-Hu 488 antibody and costained with a DNA-binding dye NucBlue show that **(A)** significant proportion of events present with detectable NucBlue-labeling and hence are annotated as nuclei. **B**, Using a Hu-unstained population of NucBlue-labeled nuclei, we create gates for Hu-immunolabeled cells, which **(C)** contain Hu-labeled nuclei in a sample that was immunolabeled with a directly conjugated Hu antibody. **D**, This population of isolated Hu- and NucBlue-labeled nuclei from adult murine small intestinal LM–MP tissues from mice from the BIDMC mouse colony, when analyzed using fluorescence intensity of NucBlue as a marker for DNA content, showed that while 88.0% of nuclei have DNA content (2N) expected in the G1 phase cells, 2.71% of Hu⁺ nuclei contain DNA content that corresponds to cells in S-phase (DNA replication phase), and 7.37% of Hu⁺ nuclei contain DNA content that corresponds to cells in G2/M phase (mitotic phase). The enumeration of nuclei does not include those that show less than 2N DNA content. **E**, Flow analysis of nuclei isolated from LM–MP of similarly aged mice housed at JHU, which were immunolabeled with anti-Hu 647 antibody postfixation and were stained with the DNA dye DAPI, shows the presence of 90.0% of nuclei have DNA content (2N) expected in the G1 phase cells, 2.61% of Hu⁺ nuclei contain DNA content that corresponds to cells in S-phase (DNA replication phase), and 7.39% of Hu⁺ nuclei contain DNA content that corresponds to cells in G2/M phase (mitotic phase). Flow analyses gates for DAPI-labeled and Hu-immunolabeled nuclei from experiment performed at JHU are shown in Extended Data Figure 3-1.

populations of pH3-immunostained cells that are present both within and outside of the myenteric ganglia (Fig. 4A,B). Importantly, using the unconjugated pH3 antibody and the anti-Hu ANNA-1 antisera, we observe that the pH3-positive, intraganglionic cell population comprises of Hu-immunostained cells (Fig. 4A,B), as well as other unlabeled cells that we assume to be populations of proliferating enteric glial cells (Zeisel et al., 2018) and enteric neuronal precursor cells, that we have previously shown to express Nestin and Ki-67 (Kulkarni et al., 2017). Using conjugated pH3 and Hu antibodies, we tested whether adult myenteric ganglia in mice housed in the barrier facility at BIDMC also similarly contained pH3-immunoreactive Hu⁺ cells (Fig. 4C). Similar to earlier observations (Kulkarni et al., 2017), CC3 immunoreactivity, which indicates apoptotic cells, was found in a subset of myenteric Hu⁺ cells (Fig. 4D). We further tested whether pH3 immunoreactivity was found both in adult murine small intestinal enteric neural precursor cells (ENPC) that express Nestin but do not express Hu and in ganglionic cells that coexpress Nestin and Hu. By coimmunolabeling, we found that pH3 immunolabeling was found both in Nestin-expressing ENPC and in Hu-expressing cells that show detectable but low expression of Nestin (Figs. 5, 6). This suggests that Hu⁺ pH3⁺ ganglionic cells are distinct from Nestin-expressing cycling ENPC.

We previously reasoned that isolated adult murine small intestinal LM–MP tissues require gentle fixation (Kulkarni and Pasricha, 2022; Kulkarni et al., 2023). To test whether the presence of pH3 in Hu⁺ ganglionic cells is an artifact of gentle fixation, we tested three additional timepoints of 10, 15, and 20 min of fixation and found that pH3 immunoreactivity was present in Hu-immunolabeled cells at each of these timepoints. Similar to our observations on binucleated Hu⁺ cells in gently fixed tissues, tissues fixed for 20 min again showed the presence of binucleated Hu⁺ cells that showed evidence of asymmetric cell division (Fig. 7).

Since coimmunolabeling with antibodies against pH3 and pan-neuronal marker Hu provides evidence of mitosis in adult small intestinal myenteric Hu⁺ cells, we next quantified the proportions of pH3-immunoreactive mitotic small intestinal

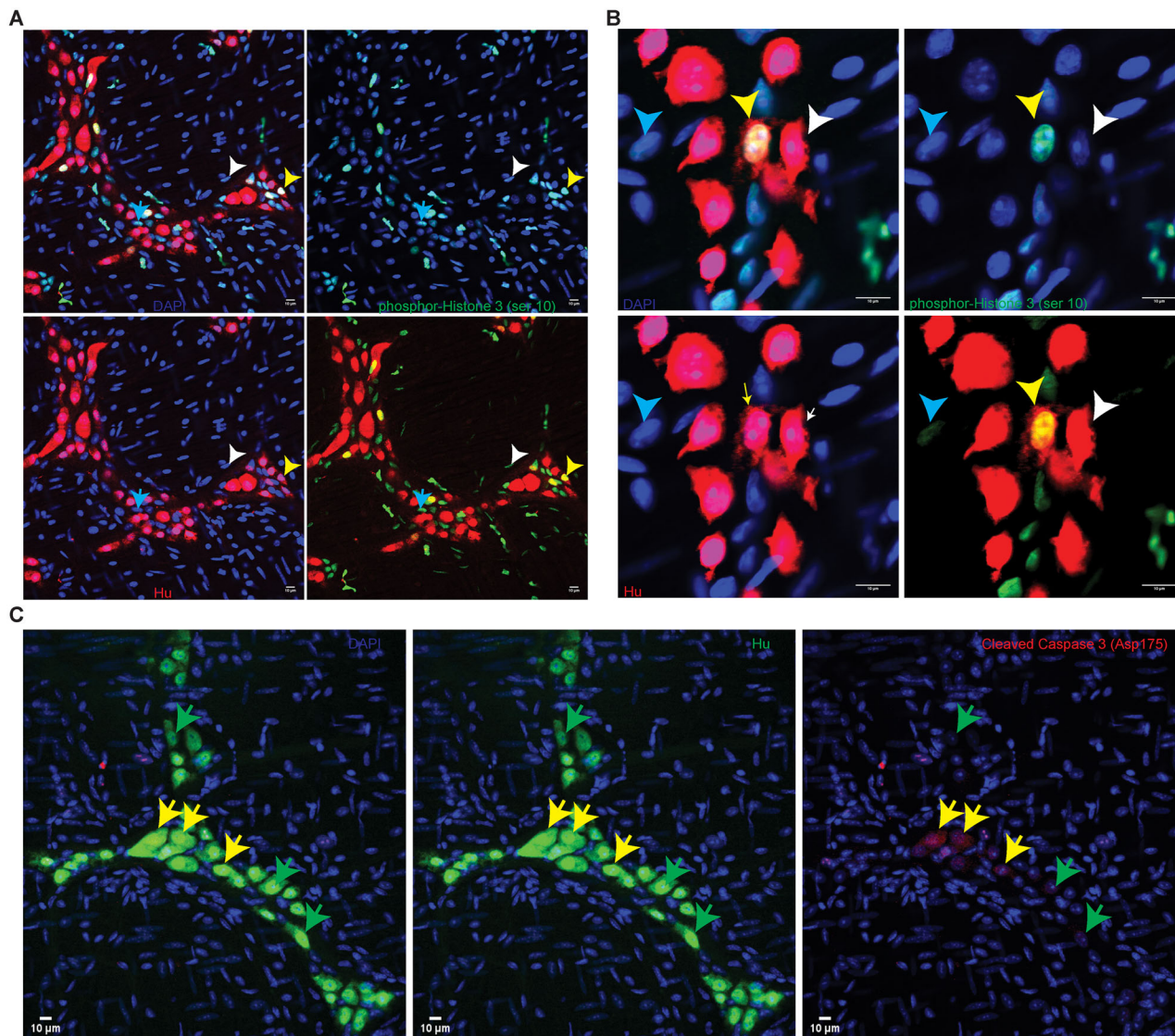


Figure 4. Cell proliferation marker pH3 is detected in neurons and other cells of the adult healthy MP tissue. Confocal microscopy shows that the (A) LM-MP tissue from an adult healthy mouse that was housed at JHU, when stained with unconjugated antibodies against pH3 (red) and the pan-neuronal marker Hu (green), shows the presence of pH3 immunoreactivity in ganglionic cells that do express Hu (yellow arrow) and those that do not express Hu (cyan arrow). pH3 immunoreactivity is also detected in extraganglionic cells in this tissue (white arrow) that are presumed to be LM cells. B, Magnified image of a myenteric ganglia labeled with antibodies against pH3 (red) and Hu (green) again shows the presence of pH3-immunoreactive Hu-immunolabeled newborn neurons (yellow arrow), along with neurons that are not immunoreactive against pH3 (white arrow) and pH3-immunoreactive extraganglionic cells (cyan arrow). C, Left, Representative image of the LM-MP tissue from an adult mouse housed in the barrier facility at BIDMC when stained with directly conjugated antibody against pH3 (red) shows the presence of significant pH3 immunoreactivity in the tissue. The tissue was also coimmunostained with directly conjugated anti-Hu antibody and the region of interest (white box) when magnified shows (right) the presence of Hu-immunolabeled (green) neurons that colabel for pH3. Nuclei are stained with DAPI (blue). D, The representative image of the adult murine small intestinal LM-MP tissue, when stained with antibodies against CC3 (red) and the pan-neuronal marker Hu (green), shows the presence of CC3 immunoreactivity in a subset of Hu-immunoreactive neurons (yellow arrows), while other neurons in the same and other ganglia do not immunolabel for CC3 (green arrow). Nuclei are labeled with DAPI (blue). Scale bar, 10 μm.

myenteric Hu^+ cells at steady state in adult mice. By confocal microscopy, we observed 2,577 Hu -immunolabeled Hu^+ cells from the small intestine of six adult healthy male and female mice ($n = 3$ of either sex), which included the MP tissue from both duodenum and ileum. We found that $8.54\% \pm 1.09$ (mean \pm SEM) of all Hu -immunolabeled cells also showed coimmunolabeling with anti-pH3 antibodies (Fig. 8A,B).

Next, we analyzed whether pH3 immunoreactivity in Hu^+ cells from ileal or duodenal myenteric ganglia showed any sex bias. In the duodenal myenteric ganglia, we counted 670 Hu^+ cells in tissues from female mice and 601 Hu^+ cells in the tissues from male mice ($n = 3$ of either sex) and found no significant difference between the percentage of pH3-immunoreactive Hu^+ cells between the two sexes (mean \pm SEM pH3 $^+$ neurons, female mice, 11.63 ± 2.00 ; male mice, 6.26 ± 0.75 ; $p = 0.17$; unpaired t test with Welch's correction; Fig. 8A). In myenteric ganglia of the ileum, we counted

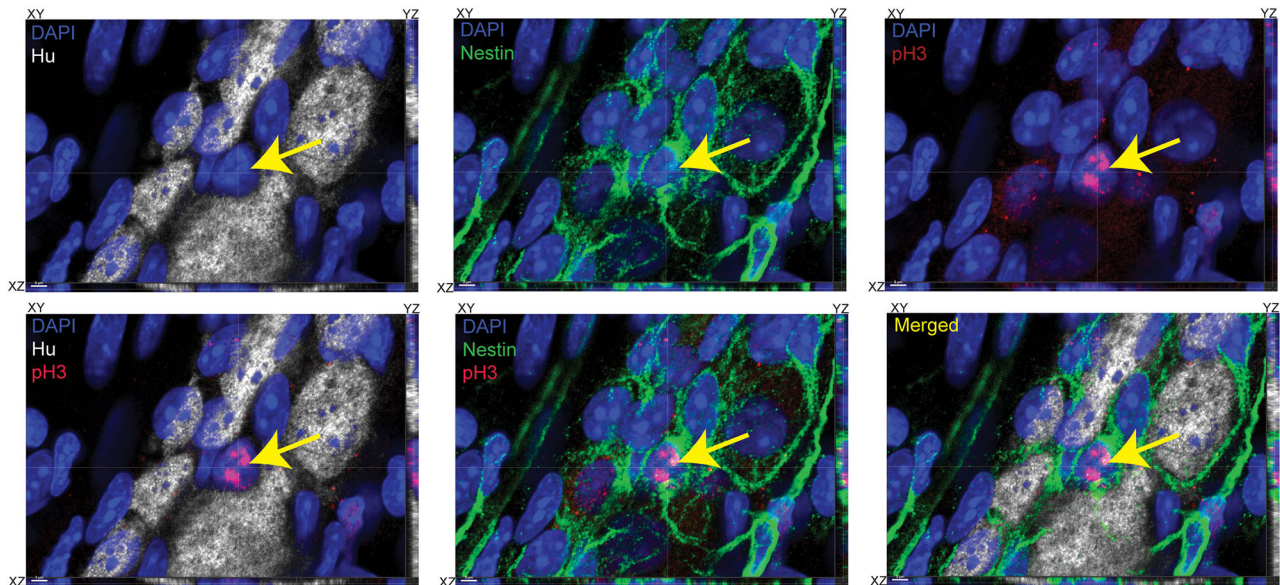


Figure 5. Nestin-expressing and Hu-nonexpressing ENPC express cell cycle marker pH3. Orthogonal (merged and color-segregated) views of a 3D confocal microscopy image showing a myenteric ganglion from an adult murine small intestinal tissue, where the tissue is immunolabeled with antibodies against Hu (gray), pH3 (red), and Nestin (green) and is stained with nuclear dye DAPI (blue). Yellow arrow points out a Nestin- and pH3-immunolabeled cell that does not immunolabel for Hu. The presence of pH3 immunoreactivity and the absence of Hu immunoreactivity in this Nestin-immunolabeled cell suggest it is a cycling enteric neural precursor cell. XY, YZ, and XY planes of the orthogonal views are denoted for every merged and panel-segregated image. Scale bar, 3 μ m.

667 Hu⁺ cells in the tissues from female mice and 639 Hu⁺ cells in the tissues from male mice ($n = 3$ of either sex) and found no significant difference between the percentage of pH3-immunoreactive Hu⁺ cells between the two sexes (mean \pm SEM pH3⁺ neurons, female mice, 9.93 ± 0.92 ; male mice, 6.82 ± 0.34 ; $p = 0.06$; unpaired t test with Welch's correction; Fig. 8B). Finally, we compared pH3 immunoreactivity in populations of Hu⁺ cells between ileal and duodenal tissue across the two sexes and found no significant difference (duodenal tissue, Hu⁺ cells counted, 1,271; mean \pm SEM pH3⁺ Hu⁺ cells, 8.64 ± 1.52 ; ileal tissue, Hu⁺ cells counted, 1,306; mean \pm SEM pH3⁺ Hu⁺ cells, 8.38 ± 0.82 ; $p = 0.88$; unpaired t test with Welch's correction; Fig. 8C).

We have previously shown that there is significant heterogeneity in ganglionic size, demonstrated by small intestinal myenteric ganglia containing as few as 3 neurons or over 100 neurons (Kobayashi et al., 2021). Here, we tested whether the proportion of mitotic Hu⁺ cells correlate with ganglionic size in the adult healthy small intestinal MP. By analyzing the proportions of pH3-immunoreactive Hu⁺ cells in 147 ganglia of various sizes (3–56 neurons per ganglia) from duodenum and ileum from six mice together, we found an absence of any significant correlation between the percentage of Hu⁺ cells immunoreactive for pH3 in myenteric ganglia and the numbers of Hu⁺ cells within ganglia (ganglionic size; D'Agonistino and Pearson's test for normality showed non-normal distribution, nonparametric Spearman correlation test, $r = -0.05625$; $p = 0.5$; Fig. 8D).

We next tested whether there was any correlation between ganglionic size and the proportions of CC3-immunoreactive apoptotic Hu⁺ cells in the adult healthy murine small intestinal MP. We quantified the percentage of CC3-immunoreactive Hu⁺ cells from 83 myenteric ganglia from three mice, where the myenteric ganglionic size ranged from 3 to 58 neurons. We found that the proportion of CC3⁺ Hu⁺ cells in small intestinal myenteric ganglia increased significantly with ganglionic size (D'Agonistino and Pearson's test for normality showed non-normal distribution, nonparametric Spearman correlation test, $r = 0.4181$; $p < 0.0001$; Fig. 8E).

Human small intestinal myenteric ganglia show evidence of neuronal turnover

We next tested whether the adult human small intestinal MP tissue also shows evidence of significant cell proliferation through the presence of pH3-immunoreactive Hu⁺ cells. In immunolabeled FFPE tissue sections, by using directly conjugated antibody against pH3, we found that many cells in the LM layer of human gut wall also showed immunoreactivity against the mitosis marker pH3 (Fig. 9A). By coimmunostaining these FFPE tissue sections with antibodies against pH3 and Hu, we found that many pH3-immunoreactive cells were found in the myenteric ganglia, some of which were also immunolabeled by antibodies against Hu (Fig. 9B). We enumerated proportions of pH3⁺ Hu⁺ cells in myenteric ganglia in FFPE tissue sections from duodenal full-thickness tissues derived from four human samples. We counted a total of 152 Hu⁺ ganglionic cells [mean \pm standard error (SE) of Hu⁺ cells counted per sample, 37.5 ± 9.56] and found that $23.43 \pm 5.22\%$ (mean \pm SE) of Hu⁺ cells is also immunolabeled for the mitosis marker pH3. These data provide evidence that significant proportions of human Hu⁺ myenteric ganglionic cells are mitotic in nature.

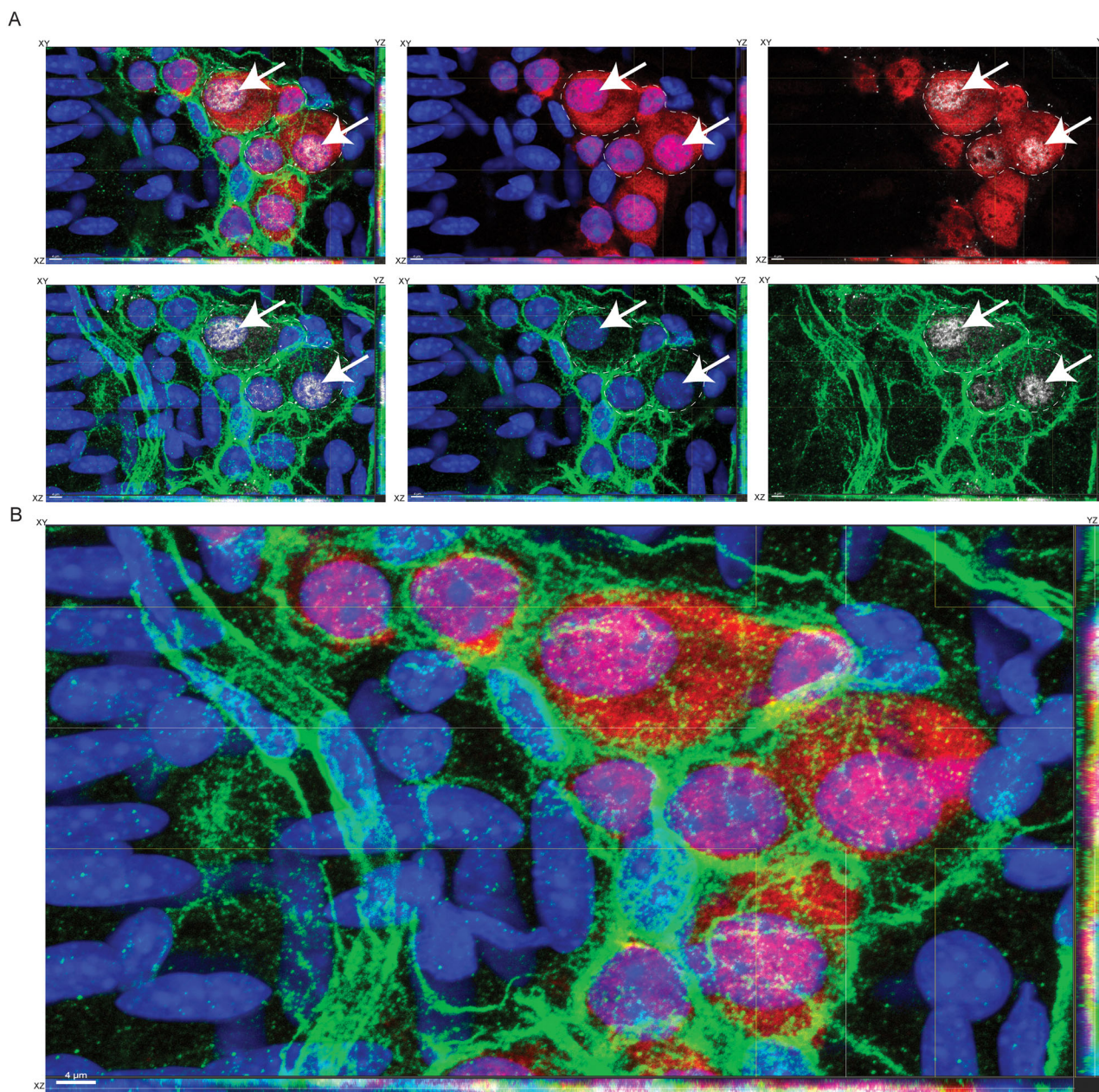


Figure 6. Hu-expressing cells that express cell cycle marker pH3 also exhibit Nestin immunoreactivity. Orthogonal (**A**) color-segregated and (**B**) color-merged image of a myenteric ganglion from an adult murine small intestinal tissue, where the tissue is immunolabeled with antibodies against Hu (red), pH3 (gray), and Nestin (green) and is stained with nuclear dye DAPI (blue). Dashed white lines depict a multinucleated contiguous Hu-immunolabeled cell, with white arrows showing that two of the three nuclei are immunolabeled with antibodies against pH3. The pH3⁺ Hu⁺ cells (white arrows) also show positive immunostaining for Nestin. XY, YZ, and XZ planes of the orthogonal views are denoted for every merged and color-segregated image. Scale bar, 4 μ m.

Similarly, we also found that the apoptotic marker CC3 was detected in a subset of human small intestinal myenteric neurons (Fig. 9C), while the negative control for CC3 immunoreactivity (performed without primary antibody) showed no background signal (Fig. 9D).

Discussion

Using established microscopic, flow cytometric, and immunolabeling-based assays (Kim et al., 2007; Kim and Sederstrom, 2015; Uguen et al., 2015; Alonso-Martin et al., 2018; An et al., 2018; Tiede et al., 2018; Jiang et al., 2019; Rotelli et al., 2019), our report provides evidence that a significant proportion of Hu⁺ ganglionic cells in the adult small intestinal MP tissue undergo mitosis. Neurogenesis from precursor cells requires DNA replication and mitosis, and the detection of mitosis and apoptosis in Hu-immunolabeled cells in healthy small intestinal MP tissue shows that there is

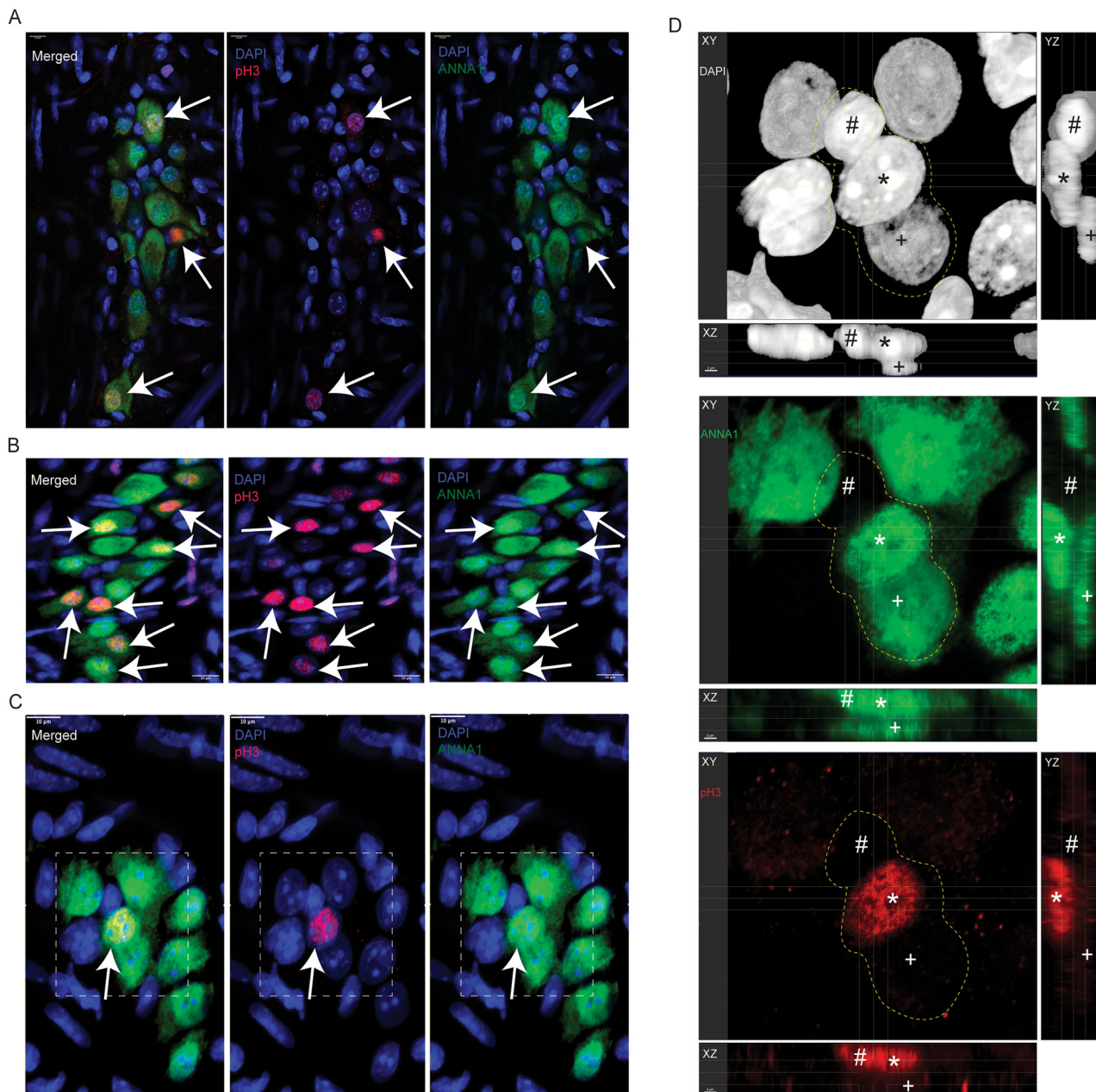


Figure 7. pH3 immunoreactivity in Hu⁺ cells is unaffected by fixation conditions. Immunostaining adult murine small intestinal LM-MP tissues that were fixed with 4% PFA for (A) 10 min, (B) 15 min, and (C) 20 min and subsequently immunostained with anti-Hu antibodies in ANNA1 serum (green) and pH3 (red) and counterstained with DAPI (blue). Merged and color-segregated views are shown for each of the treatments. White arrows show the presence of pH3 immunoreactivity in the DAPI-stained nuclei of Hu-immunoreactive cells in each of the treatments. White square in panel C is magnified in D and viewed in orthogonal views where XY, YZ, and XZ planes are shown. A contiguous nuclear structure (stained with DAPI, gray) containing three nuclear lobes “#”, “*”, “+” are observed within dashed white lines. The nuclear lobe “#” is unstained by pH3 (red) and ANNA1 (green) antibodies, lobe “*” is stained by both pH3 and ANNA1, and lobe “+” is stained by ANNA1 but not by pH3. The three panels show color-segregated views depicting an asymmetric cellular structure where parts of the nuclear structure exhibit Hu and/or pH3 immunoreactivity, while another part does not. XY, YZ, and XY planes of the orthogonal views are denoted for every merged and color-segregated image. Scale bars: A–C, 10 μm; D, 2 μm.

ongoing genesis of neurons in this organ, which offsets the continual loss of neurons to apoptosis. Our prior study, which used thymidine analog-based assays to demonstrate that almost 90% of adult small intestinal neurons were generated during a 2 week period, had suggested that ~10% of neurons are generated (and hence are newborn) on any given day (Kulkarni et al., 2017). Here, our DNA content-based flow cytometry analysis shows that ~10% of Hu-immunolabeled myenteric nuclei showed evidence of DNA content associated with G2/M (or mitotic) phase of the cell cycle. This is consistent with our microscopy-based data that demonstrate the presence of binucleate Hu⁺ cells and the immunolabeling-based data that show that ~10% of Hu-immunolabeled cells within myenteric ganglia express

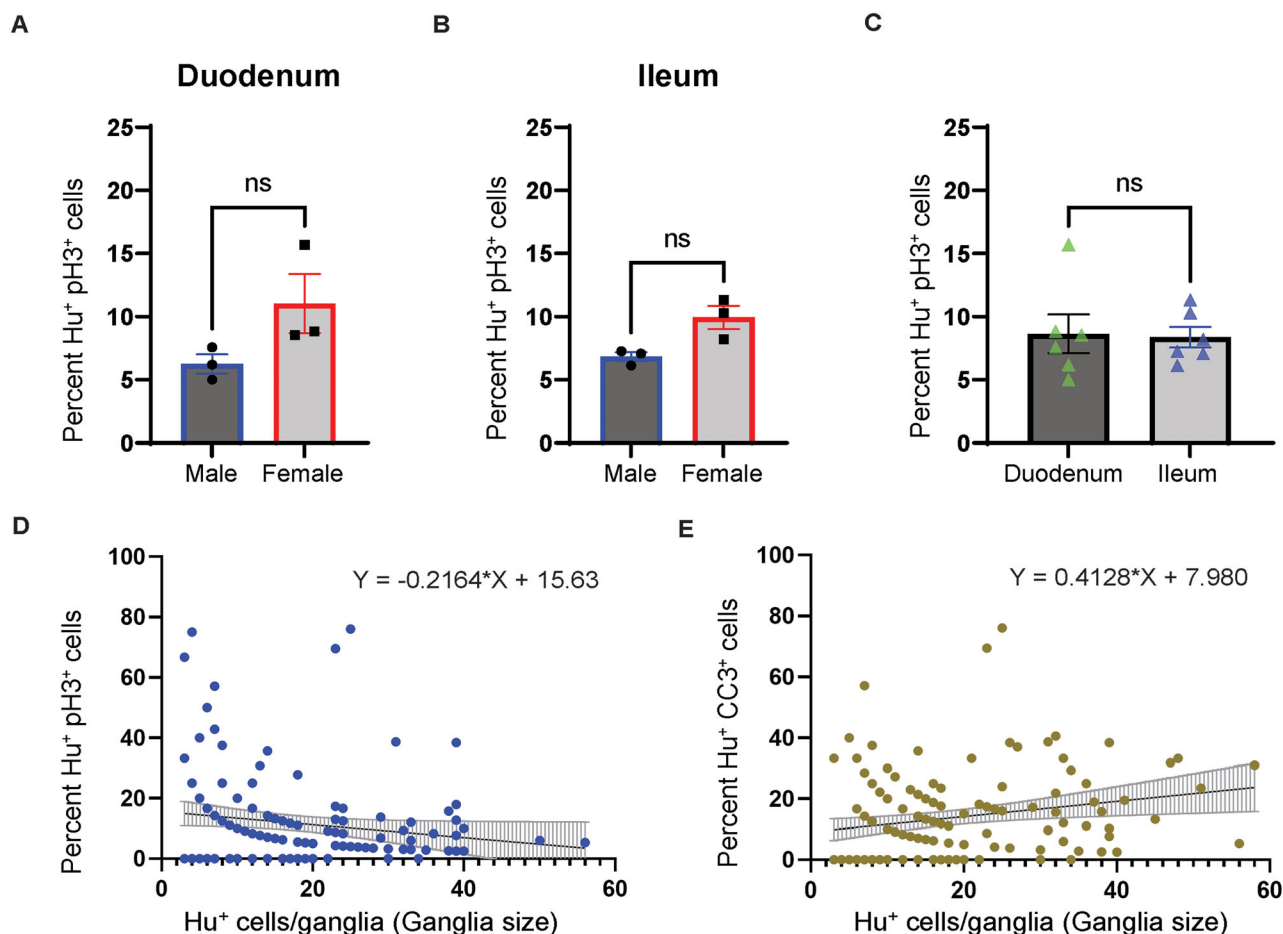


Figure 8. Quantifications of pH3-immunoreactive and CC3-immunoreactive Hu^+ cells in the adult murine gut. **A**, Quantification of pH3-immunoreactive Hu^+ cells in the duodenal tissue of age-matched male and female mice show no significant sex bias in their proportions ($p > 0.05$, Students' *t* test). **B**, Quantification of pH3-immunoreactive Hu^+ cells in the ileal tissue of age-matched male and female mice show no significant sex bias in their proportions ($p > 0.05$, Students' *t* test). **C**, Quantification of pH3-immunoreactive Hu^+ cells in the duodenal and ileal tissue of age-matched mice show no significant differences in their proportions between the two tissue regions ($p > 0.05$, Students' *t* test). **D**, Distribution of the percentage of pH3-immunoreactive Hu^+ cells in small intestinal ganglia containing various numbers of Hu^+ cells. **E**, Cubic curve fit (black line) for the distribution of CC3-immunoreactive Hu^+ cells in small intestinal ganglia containing various numbers of Hu^+ cells.

the mitotic marker pH3. Thus, our observation of ongoing mitosis in Hu -immunolabeled cells using these different methods closely matches the rate of neurogenesis we previously deduced using detection of thymidine analogs (Kulkarni et al., 2017). In addition, the presence of pH3 can be readily detected in $>20\%$ of Hu -immunolabeled ganglionic cells in the adult human gut—further suggesting that a similar neurogenic process is also present in the adult human gut. We again confirm that a subpopulation of adult murine small intestinal myenteric neurons showed detectable presence of the apoptotic marker CC3 (Kulkarni et al., 2017).

Evidence of DNA replication (S-phase) and mitosis (G2/M phase) in Hu -immunolabeled cells suggests that in addition to being a marker for mature functional neurons, Hu is also expressed by cycling neuroblasts or transit amplifying cells that are committed to a neuronal fate. Thus, rather than suggesting that adult enteric neurons are mitotic in nature, we infer that Hu immunoreactivity is not restricted to mature neurons. This argument is supported by prior studies that have shown that Hu is expressed in neuronally committed cycling progenitors or neuroblasts as well as in immature neurons (Ekonomou et al., 2015; Seki et al., 2019). The presence of a significant population of cycling Hu^+ neuroblasts in the adult MP provides evidence of a robust steady-state neurogenic process in the adult gut.

The thymidine analog-based assay we previously deployed to observe adult enteric neurogenesis requires complicated methods (Kulkarni and Pasricha, 2022). In addition, by virtue of being based on the uptake, incorporation, and accumulation of these chemicals over time into newly synthesized nucleic acids, this assay can neither sensitively measure the ongoing rate of DNA synthesis and cell proliferation at any given point of time, nor can it be used to assess the rate of neurogenesis in humans. With flow analyses, immunolabeling, and microscopy-based methods, we use simple established assays to robustly measure the proportions of cycling neuroblasts in the tissue to infer the rate of neurogenesis at health in the adult human and murine gut.

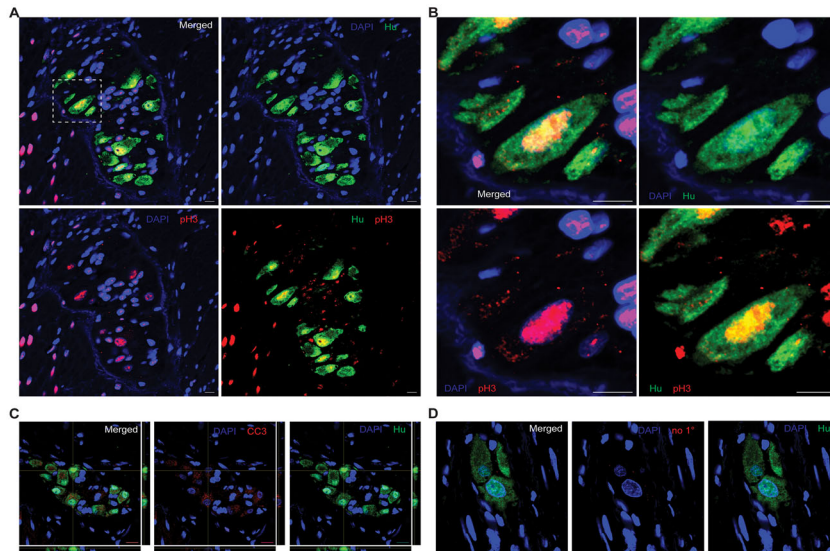


Figure 9. Hu⁺ myenteric cells expressing cell cycle marker pH3 or expressing apoptotic marker CC3 exist in human small intestinal myenteric ganglia. **A**, Cells of the LM layer of the human gut wall in FFPE tissue sections from the adult human small intestine with immunolabeling of mitotic marker pH3 (red) and costaining with DAPI (blue) show detectable pH3 immunoreactivity in many cells of this tissue. Image created by stitching contiguous 40× images of the section which was imaged with the EVOS M7000 microscope. **B**, Coimmunolabeling adjacent sections of this tissue with directly conjugated antibodies against mitotic marker pH3 (red) and pan-neuronal marker Hu (green) and by imaging them with the M7000 microscope, we observe the presence of pH3-immunoreactive cells that also immunolabel with antibodies against Hu (yellow arrows). **C**, Confocal microscopy of FFPE human tissues that were immunolabeled with anti-Hu ANNA-1 antisera and anti-pH3 antibody and then suitably costained with secondary antibodies again shows the presence of pH3 and Hu colabeled cells within the myenteric ganglia (yellow arrow). **D**, Orthogonal views generated from confocal microscopy of a myenteric ganglia immunostained with antibodies against CC3 (red) and anti-Hu ANNA-1 (green) show the presence of CC3-immunolabeled neurons. **E**, Representative image of a myenteric ganglia immunostained with antibodies against Hu (green) but no primary antibodies for the red channel shows a lack of nonspecific staining with the secondary antibodies. Photomicrographs in panels **C–E** were generated by confocal microscopy. Nuclei are labeled with DAPI (blue); scale bar, 10 μm (**C–E**).

Furthermore, two previous studies suggested that the proportions of apoptotic myenteric neurons are significantly greater in the human gut than in the murine gut (human gut 20–30% apoptotic neurons vs 10–11% in murine gut; Kozłowska et al., 2016, 2018; Kulkarni et al., 2017). Thus, it would be expected that the rate of genesis of neurons in the adult human gut would also be greater than in the murine gut. Our results, which show that ~23–24% of all human myenteric Hu⁺ cells immunolabel for the mitotic marker pH3, closely match the published rate of apoptosis in human ENS neurons. These data demonstrate that as in the murine gut, the proportions of newborn and apoptotic neurons in the human gut are evenly matched. This suggests that as established by us previously in mice, continual neurogenesis and neuronal loss are also a feature of the adult human ENS.

The immunofluorescence analyses of mitotic neuroblasts and apoptotic neurons in the murine small intestinal MP also allowed us to test whether neurogenesis occurs equally in all myenteric ganglia across two different small intestinal regions and between the two sexes. Taking the proportions of mitotic neuroblasts to mature neurons as a measure of the neurogenic activity for each ganglion, we provide evidence that neurogenic activity does not significantly differ between differently sized ganglia, between two different intestinal regions, or between sexes. However, while the rate of neurogenesis does not change across ganglia, we observe that larger ganglia (i.e., with greater number of neurons) have a higher percentage of neurons undergoing apoptosis. If neurogenesis occurs at a uniform rate across all ganglia, then the observation that apoptosis occurs more frequently in larger ganglia implies that there may be a regulatory process that discourages the preservation or further enlargement of these larger ganglia. This is reflected in our prior findings that showed that smaller ganglia are much more frequent than larger ganglia in the adult small intestinal MP tissue (Kobayashi et al., 2021). This suggests that the balance between the genesis and death of neurons within ganglia is crucial for regulating ganglionic size. Furthermore, it would indicate that any disruptions to this balance, whether through increased neurogenesis or elevated neuronal death, could alter the normal proportions of smaller and larger ganglia, potentially leading to disorders in intestinal movement. While whether such a ganglionic size-associated skew in genesis and loss of neurons extends to human tissue is still unknown, it was recently demonstrated (Boschetti et al., 2019) that patients with dysmotility have significantly reduced neuronal numbers in myenteric ganglia (or that the presence of larger ganglia in their ENS is greatly reduced). These are similar to other observations (Bernardini et al., 2012) that observed fewer numbers of myenteric neurons in patients with ulcerative colitis than in healthy controls. These observations suggest that the ganglionic rate of neurogenesis and of neuronal loss may change in disease to alter the ENS structure.

That adult enteric neurogenesis at steady state occurs in the adult ENS has been controversial (Sharkey and Mawe, 2023). Despite our prior study that observed significant proportions of label-retaining myenteric neurons in mice dosed with thymidine analogs (Kulkarni et al., 2017), other investigators were unable to replicate these findings and detect thymidine analog-based label retention in neurons (Virtanen et al., 2022). While it may be argued that the inability to detect enteric neurogenesis at steady state in the adult healthy gut may be due to technical challenges and issues (Kulkarni and Pasricha, 2022), our study furthers the case for steady-state adult enteric neurogenesis by testing the presence of DNA synthesis and mitosis in Hu-expressing myenteric cells. A recent report studied adult enteric neurogenesis at health and in disease using a different immunohistochemical marker for newborn neurons Sox2, which was also found to label ~10% of all Hu⁺ myenteric cells in the adult healthy colon (Miyata et al., 2024). The concordance between the proportions of Sox2⁺ Hu⁺ “newborn” neurons in the colon in their study and the proportions of pH3⁺ Hu⁺ myenteric cells and Hu⁺ cells in G2/M phase in our study provides evidence that myenteric neurons in the small intestine and colon do turn over in significant numbers, that the rate of neurogenesis or proportions of mitotic neuroblasts matches the observed rate of neuronal loss across various studies (Chandrasekharan et al., 2011; Nezami et al., 2014; De Schepper et al., 2018; Kulkarni et al., 2023), and that steady-state neurogenesis is an important mechanism through which adult ENS homeostasis is maintained (Kulkarni and Pasricha, 2022).

While this study furthers our model of continual neurogenesis to support neuronal homeostasis in the adult ENS, further work is needed to answer important questions that emerge considering this data and our other recent reports. One recent study provides evidence that the adult ENS consists of equal proportions of neurons derived from neural crest (NC) and mesodermal lineages (Kulkarni et al., 2023), and our prior study using thymidine analogs found that ~90% of adult enteric neurons turn over during a 2 week period (Kulkarni et al., 2017). The near-comprehensive nature of neuronal turnover in the adult ENS suggests that in addition to genesis of NC-derived enteric neurons, which we showed occurs from Nestin-expressing NC-derived precursor cells, the population of mesoderm-derived enteric neurons (MENs) also turn over at steady state. While our report found molecular evidence of continual genesis of MENs in the postnatal ENS (Kulkarni et al., 2023), this current report does not test the identity of precursor cells for the MEN lineage or the proportions of mitotic neuroblasts of the two different lineages. Future work will focus on establishing how ganglionic Hu⁺ cells of the mesodermal and NC-lineage differ in their proportions of cycling cells at different ages. In addition, our microscopic assessment of myenteric ganglia provides evidence of binucleated cells and of pH3-immunolabeled Hu⁺ cells that appear to undergo asymmetric division into Hu^{-/+} cells. Mechanisms of cell division include canonical nucleokinesis and cytokinesis, as well as noncanonical endoreduplication and closed mitosis, through which cells may increase their nuclear DNA content without cytokinesis or maintain their nuclear membranes while undergoing cytokinesis (Shu et al., 2018; Rotelli et al., 2019; Dey et al., 2020). While the presence of asymmetric Hu-immunolabeled cells, where cell structure shows varying immunolabeling for Hu and pH3, suggests the presence of noncanonical cytokinetic mechanisms in the adult ENS, the nature of the precise cell biological mechanisms through which Hu⁺ cells cycle need to be further interrogated in detail. This study provides the rationale for studying these mechanisms in the future.

Our study is robust as it establishes concordance of our observations through different approaches—the high-resolution microscopy approach to test the presence of binucleated Hu-expressing cells, DNA content-based flow analyses to test the presence of diploid DNA content indicative of S- and G2/M phase, and the pH3-based immunofluorescence assay-based approach to identify and enumerate the proportions of mitotic Hu-expressing cells in adult murine and human ENS. Thus, this study further confirms the presence of the homeostatic mechanism of steady-state neuronal turnover in the adult ENS.

References

- Alonso-Martin S, Auradé F, Mademtoglou D, Rochat A, Zammit PS, Relaix F (2018) SOXF factors regulate murine satellite cell self-renewal and function through inhibition of β -catenin activity. *Elife* 7:e26039.
- An Z, Sabalic M, Bloomquist RF, Fowler TE, Streebman T, Sharpe PT (2018) A quiescent cell population replenishes mesenchymal stem cells to drive accelerated growth in mouse incisors. *Nat Commun* 9:378.
- Becker L, Nguyen L, Gill J, Kulkarni S, Pasricha PJ, Habtezion A (2018) Age-dependent shift in macrophage polarisation causes inflammation-mediated degeneration of enteric nervous system. *Gut* 67:827–836.
- Bernardini N, et al. (2012) Immunohistochemical analysis of myenteric ganglia and interstitial cells of Cajal in ulcerative colitis. *J Cell Mol Med* 16:318–327.
- Boschetti E, et al. (2019) Enteric neuron density correlates with clinical features of severe gut dysmotility. *Am J Physiol Gastrointest Liver Physiol* 317:G793–G801.
- Chandrasekharan B, Anitha M, Blatt R, Shahnavaz N, Kooby D, Staley C, Mwangi S, Jones DP, Sitaraman SV, Srinivasan S (2011) Colonic motor dysfunction in human diabetes is associated with enteric neuronal loss and increased oxidative stress. *Neurogastroenterol Motil* 23:131–138.e26.
- D’Errico F, et al. (2018) Estrogen receptor beta controls proliferation of enteric glia and differentiation of neurons in the myenteric plexus after damage. *Proc Natl Acad Sci U S A* 115:5798–5803.
- De Schepper S, et al. (2018) Self-maintaining gut macrophages are essential for intestinal homeostasis. *Cell* 175:400–415.e13.
- Desmet A-S, Cirillo C, Vanden Berghe P (2014) Distinct subcellular localization of the neuronal marker HuC/D reveals hypoxia-induced damage in enteric neurons. *Neurogastroenterol Motil* 26:1131–1143.
- Dey G, Culley S, Curran S, Schmidt U, Henriques R, Kukulski W, Baum B (2020) Closed mitosis requires local disassembly of the nuclear envelope. *Nature* 585:119–123.
- Ekonomou A, et al. (2015) Stage-specific changes in neurogenic and glial markers in Alzheimer’s disease. *Biol Psychiatry* 77:711–719.

- Gregersen H, Kassab G (1996) Biomechanics of the gastrointestinal tract. *Neurogastroenterol Motil* 8:277–297.
- Hamnett R, Dershowitz LB, Sampathkumar V, Wang Z, Gomez-Frittelli J, De Andrade V, Kasthuri N, Druckmann S, Kaltschmidt JA (2022) Regional cytoarchitecture of the adult and developing mouse enteric nervous system. *Curr Biol* 32:4483–4492.e5.
- Hyland NP, Cryan JF (2016) Microbe-host interactions: influence of the gut microbiota on the enteric nervous system. *Dev Biol* 417:182–187.
- Jiang YH, Zhu Y, Chen S, Wang HL, Zhou Y, Tang FQ, Jian Z, Xiao YB (2019) Re-enforcing hypoxia-induced polyploid cardiomyocytes enter cytokinesis through activation of beta-catenin. *Sci Rep* 9:17865.
- Kim Y-J, Ketter R, Steudel W-I, Feiden W (2007) Prognostic significance of the mitotic index using the mitosis marker anti-phosphohistone H3 in meningiomas. *Am J Clin Pathol* 128:118–125.
- Kim KH, Sederstrom JM (2015) Assaying cell cycle status using flow cytometry. *Curr Protoc Mol Biol* 111:28.6.1–28.6.11.
- Kobayashi Y, et al. (2021) COUNTEN, an AI-driven tool for rapid and objective structural analyses of the enteric nervous system. *eNeuro* 8:ENEURO.0092-0021.2021.
- Kozłowska A, Kozera P, Majewski M, Godlewski J (2018) Co-expression of caspase-3 or caspase-8 with galanin in the human stomach section affected by carcinoma. *Apoptosis* 23:484–491.
- Kozłowska A, Kwiatkowski P, Oponowicz A, Majewski M, Kmiec Z, Godlewski J (2016) Myenteric plexuses atrophy in the vicinity of colorectal cancer tissue is not caused by apoptosis or necrosis. *Folia Histochem Cytobiol* 54:99–107.
- Kulkarni S, et al. (2017) Adult enteric nervous system in health is maintained by a dynamic balance between neuronal apoptosis and neurogenesis. *Proc Natl Acad Sci U S A* 114:E3709–E3718.
- Kulkarni S, et al. (2023) Age-associated changes in lineage composition of the enteric nervous system regulate gut health and disease. *Elife* 12:RP88051.
- Kulkarni S, Pasricha PJ (2022) Detecting adult enteric neurogenesis in the context of adult ENS homeostasis. *Cell Mol Gastroenterol Hepatol* 14:967.
- Liu MT, Kuan YH, Wang J, Hen R, Gershon MD (2009) 5-HT4 receptor-mediated neuroprotection and neurogenesis in the enteric nervous system of adult mice. *J Neurosci* 29:9683–9699.
- Miyata K, Yamamoto T, Kato R, Hayashi S, Kadowaki M (2024) Preferential neurogenesis of nitrergic neurons in the myenteric plexus of the DSS-induced colitis mouse colon causes colonic dysmotility in colitis. *Am J Physiol Gastrointest Liver Physiol* [Epub ahead of print].
- Nezami BG, Mwangi SM, Lee JE, Jeppsson S, Anitha M, Yarandi SS, Farris AB 3rd, Srinivasan S (2014) MicroRNA 375 mediates palmitate-induced enteric neuronal damage and high-fat diet-induced delayed intestinal transit in mice. *Gastroenterology* 146:473–483.e3.
- Panet E, Ozer E, Mashriki T, Lazar I, Itzkovich D, Tzur A (2015) Purifying cytokinetic cells from an asynchronous population. *Sci Rep* 5:13230.
- Rotelli MD, Policastro RA, Bolling AM, Killion AW, Weinberg AJ, Dixon MJ, Zentner GE, Walczak CE, Lilly MA, Calvi BR (2019) A cyclin a-Myb-MuvB-Aurora B network regulates the choice between mitotic cycles and polyploid endoreplication cycles. *PLoS Genet* 15:e1008253.
- Seki T, Hori T, Miyata H, Maehara M, Namba T (2019) Analysis of proliferating neuronal progenitors and immature neurons in the human hippocampus surgically removed from control and epileptic patients. *Sci Rep* 9:18194.
- Sharkey KA, Mawe GM (2023) The enteric nervous system. *Physiol Rev* 103:1487–1564.
- Sherman MP, Zaghoulani H, Niklas V (2015) Gut microbiota, the immune system, and diet influence the neonatal gut-brain axis. *Pediatr Res* 77:127–135.
- Shu Z, Row S, Deng WM (2018) Endoreplication: the good, the bad, and the ugly. *Trends Cell Biol* 28:465–474.
- Tiede S, et al. (2018) The FAK inhibitor BI 853520 exerts anti-tumor effects in breast cancer. *Oncogenesis* 7:73.
- Uguen A, Conq G, Doucet L, Talagas M, Costa S, De Braekeleer M, Marcourelles P (2015) Immunostaining of phospho-histone H3 and Ki-67 improves reproducibility of recurrence risk assessment of gastrointestinal stromal tumors. *Virchows Arch* 467:47–54.
- Virtanen H, Garton DR, Andressoo J-O (2022) Myenteric neurons do not replicate in small intestine under normal physiological conditions in adult mouse. *Cell Mol Gastroenterol Hepatol* 14:27–34.
- Ye L, et al. (2020) Caspase-11-mediated enteric neuronal pyroptosis underlies western diet-induced colonic dysmotility. *J Clin Invest* 130:3621–3636.
- Zeisel A, et al. (2018) Molecular architecture of the mouse nervous system. *Cell* 174:999–1014.e22.